Characterization of an Electron Gun for Hollow Electron Beam Collimation

Siqi Li*
University of Chicago

Giulio Stancari (supervisor)
Fermi National Accelerator Laboratory, P.O. Box 500, Batavia, Illinois 60510, USA

(Dated: August 6, 2012)

Hollow electron beam collimation (HEBC) is a new technique developed to complement conventional beam collimation system to remove beam halo in a controlled fashion. We study the characteristics of the electron gun that produces the hollow electron beam. Cathode yield and beam profile measurements are used to extract information on gun performance. Results of characteristic measurements are presented.

*E-mail: lisiqi@fnal.gov

Contents

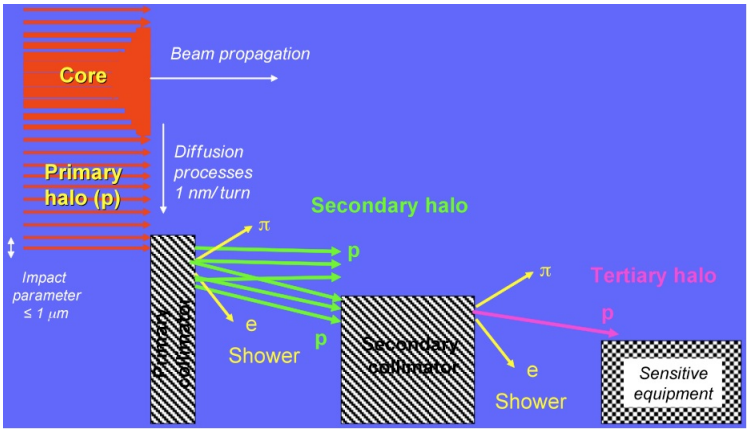

FIG. 1: Mechanism of conventional collimator system. Photo by R. Assmann.

I. INTRODUCTION

We are studying hollow electron beam as a new technique of collimation system used for high-intensity beams in storage rings and colliders. Detailed description can be found at Ref [B] Collimation system is important in high-energy particle accelerators and storage rings, because it protects equipment from damage due to particle aborts. It is used for controlling and reducing beam halo, which is continuously produced by processes such as beam-gas scattering, intrabeam scattering, electrical noise in the accelerating cavities, ground motion, betatron resonances, and beam-beam collision. Beam halo is undesirable because it is a potential cause for unwanted radioactivity and a source of experimental backgrounds. Therefore, it is of great interest to develop an effective collimation technique that removes the beam halo.

Conventional collimation system consists mainly of two-stage collimators, possibly followed by several successive stages. They are formed by a primary collimator (the target) and a secondary collimator (the absorber). The basic mechanism of a two-stage collimator is shown in Figure 1. The primary collimator is the device that is closest to beam core and generates random transverse kicks via multiple Coulomb scattering. For example, in the Tevatron, the primary collimators are 5-mm tungsten plates placed about 5 standard deviations (σ) away from the beam core. The random multiple-scattering kick has a root mean square of 17 μrad for 980-GeV protons. The secondary collimator is placed farther away from the beam core than the primary. The affected particles from the primary stage, as well as the newly-produced particles from the primary collimator, get absorbed by the secondary collimator. In the Tevatron, the secondary collimators are 1.5-m steel blocks placed at 6σ away from the beam core. If necessary, more collimators are placed following the secondary collimator to increase the absorption efficiency.

The conventional two-stage collimation system effectively shields sensitive equipment from beam aborts, and reduces beam-related background in experiments. However, it has two main limitations. First,

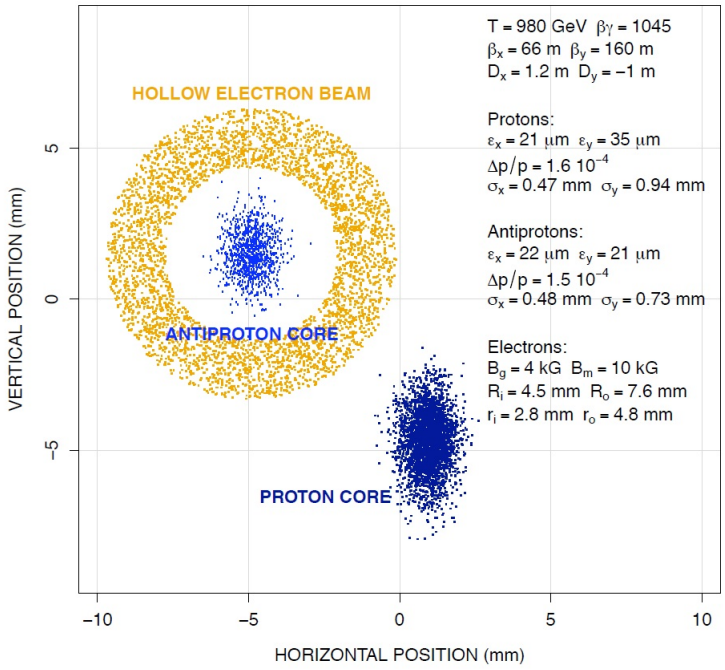

FIG. 2: Example of hollow electron beam layout in the Tevatron (photo by G. Stancari.)

in a high-energy particle accelerator, no material can be placed too close to the beam. Placing the collimator too close to the beam results in increased beam loss rates and radiation damage. The electromagnetic impedance of the collimator also gives some constraints. Another problem is beam jitter. The beam oscillates as a result of mechanical vibrations, such as ground motion. Even with active orbit stabilization, the beam centroid may oscillate by tens of microns. This translates into periodic bursts of losses at aperture restrictions.

To address these limitations, we are studying hollow electron beam as a new collimation technique. In a hollow electron beam collimator (HEBC), electrons enclose the circulating beam immersed in a solenoidal field (Figure 2). The electron beam is generated by a pulsed electron gun, which is transported with strong axial magnetic fields, in an arrangement similar to electron cooling and electron lenses. Because of its low impedance, we can place HEBC very close to the circulating beam and even overlap with it, and it does not lead to any material damage. In addition, the effect of HEBC on the main circulating beam reduces the beam sensitivity to surrounding vibration.

The electric charge of the electrons kicks halo particles transversely according to the following equation:

$$\theta = \frac{2I_r L(1 \pm \beta_e \beta_p)}{r\beta_e \beta_p c^2 (B\rho)_p} \left(\frac{1}{4\pi\varepsilon_0} \right), \tag{1}$$

where I_r is the beam current, L is the length the beam travels, $B\rho$ is the proton beam rigidity, ε_0 is the vacuum permittivity, $\beta_e c$ is the electron velocity, and $\beta_p c$ is the particle velocity. The + sign indicates that

the magnetic force and electric force are in the same direction. For typical parameters, the kick given to a 980-GeV protons is on the order of 0.2 μrad.

Several measurements have been done in Fermilab Tevatron to test the compatibility of HEBC with collider operations, acting on the antiproton beam. The effects of HEBC on antiproton beam includes scraping the beam halo while leaving the beam core unperturbed, increasing halo diffusion rate, and removing the correlation between beam losses from diffeent bunch trains and hence reducing sensitivity to beam jitter. Detailed description and data analysis of such studies can be found in Ref [B].

This project focuses on characterizing a new, 1-inch-diameter electron gun, for possible use at CERN in the LHC or SPS machine. The major goal of this project is to test the feasibility of a larger and more powerful gun than that tested at Fermilab Tevatron. The cathode yield as a function of voltage and temperature and the electron beam profile are of particular interest. They provide a tool for diagnosing the performance of the cathode and understanding its geometry and operation, so that we have better control over the produced pulsed electrons. In addition, we analyzed our data according to Longo's model describing the transition between current densities in different regimes, which is important in diagnosing the surface uniformity of the emitter. In this paper, we present the characteristics of the hollow electron beam at the Fermilab electron lens test stand.

II. PRINCIPLES OF THERMIONIC ELECTRON GUNS

We use a thermionic dispenser cathode as our source of electrons. A thermionic dispenser cathode is a device that emits electrons according to thermionic emission mechanism. As we increase the temperature of cathode surface, electrons in the cathode can escape from the surface of the cathode when the energy gained from heating reaches a certain value. The threshold energy above which electrons are thermally excited to escape the cathode is the sum of *Fermi level energy* and *work function*, $E_0 + e\phi$. Work function is determined by the cathode material.

Using Fermi-Dirac distribution and appropriate approximations, we can arrive at Richardson-Dushman equation to describe the relation between emission current density and temperature of a cathode with no applied electric field:

$$J = A_0 T^2 e^{-\frac{e\phi}{kT}}, \tag{2}$$

where A_0 is a universal constant and has a value 1.20×10^6 A/m^{2}K^2. Detailed derivation can be found at Ref [B]. When the cathode is used, we place an anode at a higher electric potential in conjunction with the cathode. The presence of the anode creates an electric field, whose effect is not considered in the

Richardson-Dushman equation. To include the effect of the applied electric field on an emitted electron, we consider the increase in its kinetic energy as the electron moves in between the cathode and the anode. The increase in kinetic energy is the same as the corresponding decrease in potential energy. In addition to the applied field, the emitted electron induces an image charge in the cathode, which creates a surface field via the Coulomb force between the emitted electron and the image charge. Therefore the total electric field experienced by the emitted electron is the sum of the applied field and the surface field. The effect of the applied field is called the *Schottky effect*. Taking Schottky effect into account, we can correct Richardson-Dushman equation as follows,

$$J = A_0 T^2 e^{-\frac{e}{kT}[\phi - \sqrt{\frac{eE_a}{4\pi\varepsilon_0}}]}, \tag{3}$$

where E_a is the electric field strength between the cathode and the anode.

The above analysis addresses the relation between emission current density and temperature. This regime is called *temperature limited* (TL) regime. However, as the voltage increases, the cathode will reach its *full space-charge limit* (FSCL) regime, where increasing temperature does not affect the emission current. The space-charge effect is a result of the negative charge of electrons, which reduces the potential energy at the surface of the cathode. This limit occurs when the density of electrons adjacent to the cathode surface becomes so large that the potential energy reduces below zero and the electrons are forced to flow back to the cathode. In this regime, we study the relation between emission current in relation to cathode-anode voltage. Applying energy conservation law and Poisson's equation, we can get the relation between emission current and voltage as follows,

$$I = PV^{\frac{3}{2}}, \tag{4}$$

where P is known as the *perveance* of the diode. This is called the Child-Langmuir law. For example, for a parallel plate diode,

$$P = \frac{4}{9}\frac{A\varepsilon_0}{d^2}\sqrt{\frac{2e}{m_e}}, \tag{5}$$

where A is the area of cathode, d is the distance between cathode and anode, and m_e is the mass of the electron. Perveance is a function only of the geometry of the diode, and therefore it is a useful tool in diagnosing the cathode geometry, which is addressed below in Section [IV].

To describe the transition of the emission curve from one regime to the other, Longo proposed a model addressing this issue [B]. The basic model is

$$\frac{1}{J} = \frac{1}{J_{sc}} + \frac{1}{J_{tl}}, \tag{6}$$

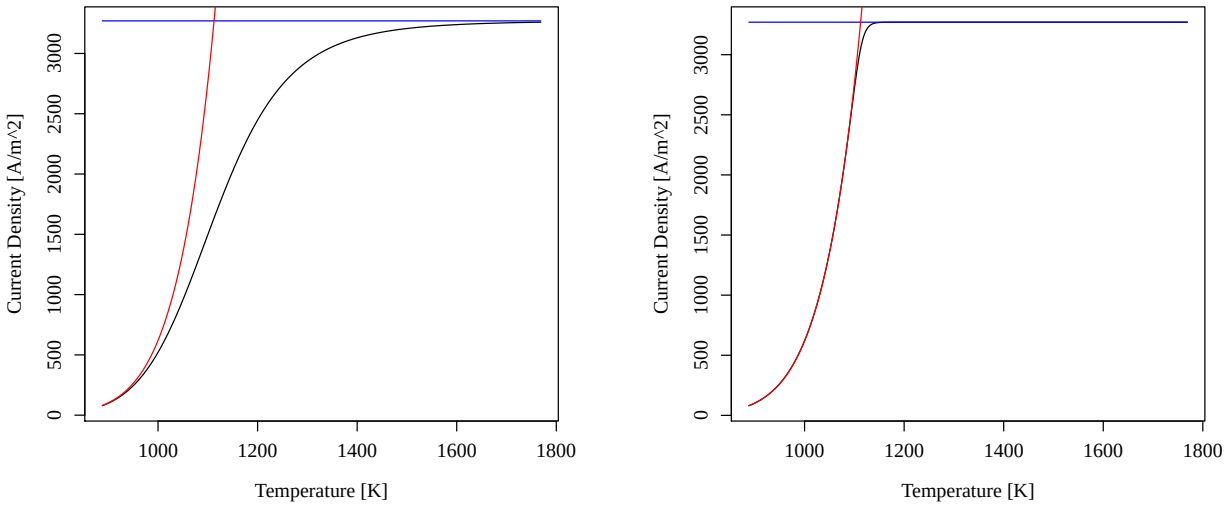

FIG. 3: Example of the effect of shape factor. Cathode-anode voltage at 7000 V, shape factor α=1 (left) and shape factor α=10. J (black), J_{sc} (blue), J_{tl} (red).

where J is the observed current density, J_{sc} is the theoretical current density in space-charge limited regime, and J_{tl} is the theoretical current density in temperature-limited regime. In Longo's paper, he discusses the change of the emission curve shape as time goes on. He adopts Vaughan's suggestion [B] to raise each term of Equation 6 to a power α, known as the *shape factor*. The modified equation is

$$\frac{1}{J^{\alpha}} = \frac{1}{J_{sc}^{\alpha}} + \frac{1}{J_{tl}^{\alpha}} \tag{7}$$

The α is called a shape factor because it is related to the uniformity of the emitter surface. It has been generally accepted that the more uniform the emitter surface is, the sharper the transition of the emission curve is. Figure 3 illustrates how the change in the shape factor α changes the transition of the emission curve.

III. ELECTRON LENS TEST STAND

The electron lens test stand is located in Fermilab lower linac gallery. It was originally developed for Tevatron electron lens, but now it is also used for testing hollow electron beam. The main experimental apparatus consists of a pulsed electron gun, a straight beamline, and a collector. The vacuum beam line is surrounded by three solenoids. Figure 4 shows a photograph of the main apparatus. The three solenoids are called, from left to right in Figure 4, the gun solenoid, the main solenoid, and the collector solenoid. Figure 5 shows the layout of the howllow electron beam and the antiproton beam in the Tevatron electron lens.

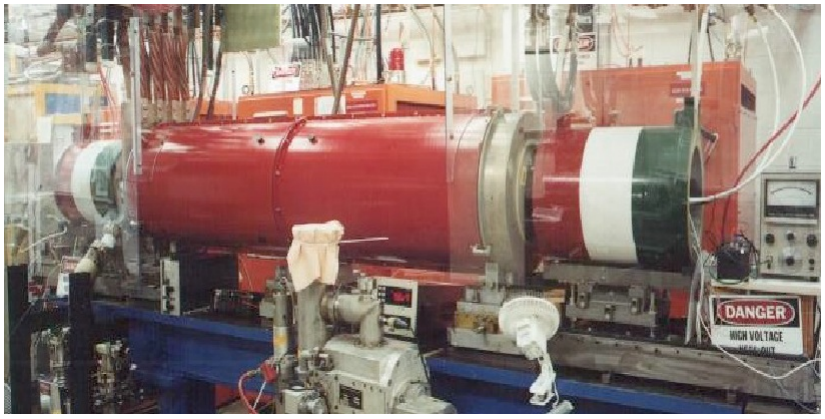

FIG. 4: Electron lens test stand at Fermilab lower linac gallery.

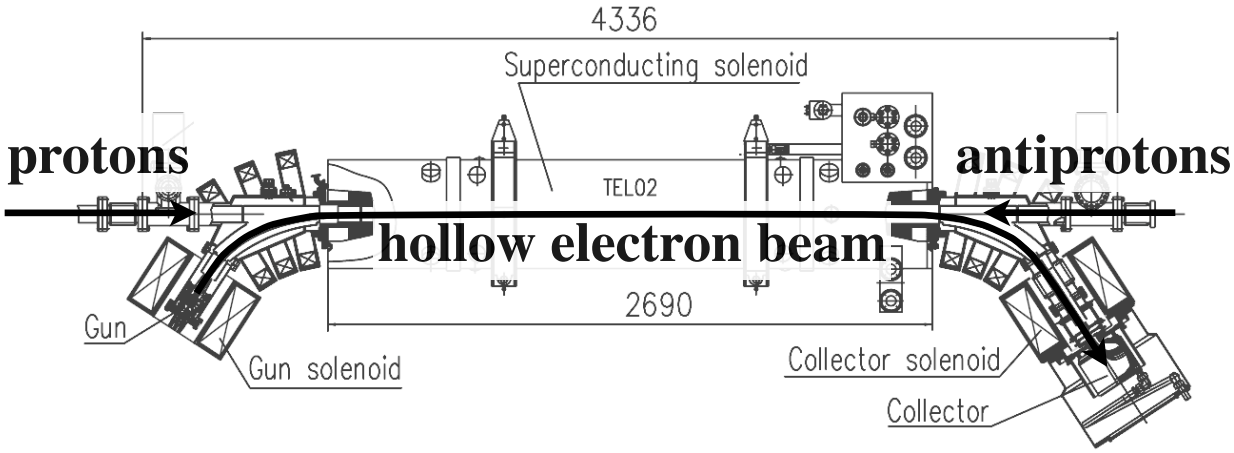

FIG. 5: Layout of the beams in the Tevatron.

The gun solenoid goes around the electron gun. For a typical magnetic strength of 0.3 T, the current in the coil in the gun solenoid is approximately 1800 A. The main solenoid needs four times the current in the coil to provide a 0.3 T magnetic field. The 3-m straight beamline is equipped with pickup electrodes. The electron collector is installed in the collector solenoid. The current in the collector solenoid runs at 1800 A to provide a 0.3 T magnetic field. The collector has a 0.2-mm-diameter pinhole for current-density profile measurements, which are detailed below. This configuration is usually referred to as a "3-3-3 kG configuration". A 18-MOhm low-conductivity cooling water circuit provides cooling for the power supplies, solenoids, and the collector.

The vacuum environment in the beamline is provided by two pumping systems. The primary one is a fore vacuum, Oerlikon Leybold Turbolab 80 (turbo+diaphragm). The secondary one is a high vacuum which consists of three ion pumps. The ion pumps are connected to the vacuum chamber for the beam.

The fore pump is connected to the high pump through a valve. We first open the valve and use only the turbo+diaphragm pump to reduce the pressure down to 10^{-6} mbar. Then we close the valve and use only the ion pumps to reduce the pressure further down to 10^{-8} mbar.

To characterize the electron gun, we mainly studied the cathode yield and beam profile. The cathode yield describes the relation between the yield current and the cathode-anode voltage. Electrons are produced in pulses from the electron gun. The pulse width and the period of the electron gun is monitored by an oscilloscope to accommodate the high voltages and peak currents of the electron gun. Different settings of the pulse width and pulse period allow us to achieve different high voltage and peak current. The yield current was read out from the output of the collector. The output current goes through two toroids, which measure the voltage across each toroid. The output is displayed on an oscilloscope as a voltage pulse with relation to time. The voltage was measured as the average amplitude voltage of the pulse. This voltage is calibrated against yeild current such that 1 V corresponds to 1 A collector current. Thus, we were able to measure the collector current.

Current density profile is measured by recording the current through the collector pin hole while sweeping the electron beam with the magnetic correctors in small steps. A software has been developed to monitor the run throughout the measurement. Examples of profile measurements are given in Section [IV] below.

IV. 1-INCH HOLLOW ELECTRON GUN

A. Main Features

A high-perveance gun was developed to emit hollow electron beam. A tungsten dispenser cathode with BaO:CaO:Al_2O_3 impregnant is used to obtain high perveance and appropriate work function. Theoretically, the tungsten melting point is 3410 °C, and the work function is 4.6 eV. For barium, the melting point is 725 °C, and the work function is 2.7 eV. When the cathode is heated for a long enough time, typically after a few hours, the barium diffuses into the pores on the tungsten surface, and hence decreases the effective work function.

B. Design Considerations

To approximately determine the required size of the hollow electron gun, weconsidered typical LHC parameters. The energy of the protem beam is 7 TeV, corresponding to a Lorentzian γ_r approximately 7×10^3. The beam size is calculated using the transverse amplitude function, which is approximately $\beta = 200\ m$, and the transverse normalized emittance, which is approximately $\varepsilon = 2\ \mu$m. The transverse

beam size is therefore

$$\sigma = \sqrt{\frac{\beta\varepsilon}{\gamma_r}} = \sqrt{\frac{200m \cdot 2 \times 7 \times 10^{-6}m}{10^3}} \approx 0.3\ mm. \tag{8}$$

Assuming the beam follows a Gaussian distribution transversely, the beam core is within $3\sigma \approx 0.9\ mm$. The hollow electron beam should span 4σ to 8σ, corresponding to 1.2 mm to 2.4 mm. The above dimension applies to the main solenoid, where the magnetic field strength should be larger than 1 T for stability and smaller than 6 T due to technological limitations. Similarly, in the gun solenoid, the appropriate magnetic field strength is larger than 0.2 T and smaller than 0.4 T, creating a one-order-of-magnitude difference between the main solenoid and gun solenoid magnetic field strength. However, the flux of the magnetic field remains constant for both the main and gun solenoids. Therefore, the radius of beam in the gun solenoid, r_{gun}, and the radius of beam in the main solenoid, r_{main}, should follow this relation:

$$r_{gun} = r_{main}\sqrt{\frac{B_{gun}}{B_{main}}}, \tag{9}$$

where B_{gun} and B_{main} are the respective magnetic field strength in the gun and main solenoids. Thus we can get $r_{gun} \approx 6\ mm$, with a diameter of 12 mm. Note that we have neglected the effect of dispersion due to the beam momentum spread. If we were to take dispersion into account, the beam size would be $x^2 = (D\frac{\Delta p}{p})^2 + \sigma^2$. For the LHC, we consider the hollow electron beam dispersion D $\approx$ 1 m, and the momentum spread $\frac{\Delta p}{p} \approx 1.5 \times 10^{-4}$. So, $x^2 = 10^{-8}m^2 + 10^{-5}m^2$, and we can see that the first term is negligible.

Figure 6 shows the longitudinal cross section of the 1-inch hollow electron gun. The outer diameter of the cathode is 25.4 mm (1 in). The diameter of the hole is 13.5 mm, consistent with our calculation using LHC parameters. The electrodes around the cathode help focus the electron beam. Figure 7 is a photograph of the cathode, which is the tungsten hollow cylinder in the middle.

C. Perveance Measurement

The perveance, as introduced above, relates the gun yield current to the cathode-anode voltage. We measured the perveance over a large range of temperature and voltage. The pulse width and the period of the electron gun is monitored by an oscilloscope to accommodate the high voltages and peak currents of the electron gun. Different settings of the pulse width and pulse period allow us to achieve different high voltage and peak current. Figure 8 shows an example of the pulse shape on oscilloscope. The purple curve shows the pulse of the electron beam from the voltage modulator, and the green curve shows the pulse measured by the toroid at the collector solenoid. We took the amplitude of the green curve as the cathode yield current.

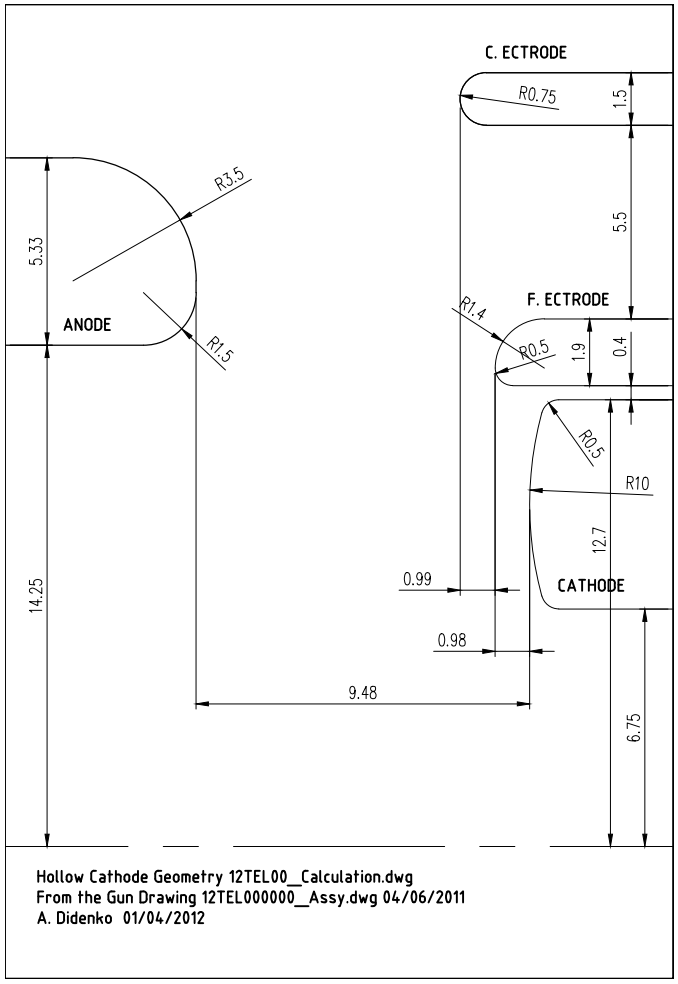

FIG. 6: 1-Inch Hollow Gun Dimensions

FIG. 7: Cathode of the 1-inch hollow electron gun

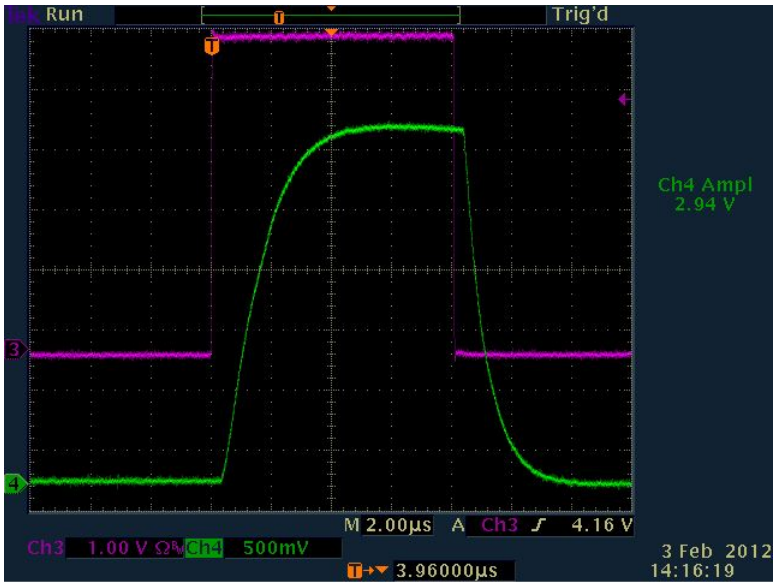

FIG. 8: Example of pulse shape shown on oscilloscope for perveance measurement

We have taken two sets of data to study cathode perveance. One was taken from December, 2011 to February, 2012. The other was taken in June, 2012. Our results show that these two data sets are consistent with each other.

Figure 9 compares the two data sets. Data points were taken when the heating filament current equals 8.75 A, corresponding to cathode temperature at approximately 1100 °C. The uncertainty in current was calculated by adding a constant uncertainty of 0.05 mA in reading from the oscilloscope, an estimate of measurement uncertainty of 0.1%, and a systematic uncertainty of 1 mA in quadrature. The uncertainty in voltage is negligible. The least square fit is weighted by the square of uncertainty reciprocal. The earlier data set shows a perveance of $(4.24 \pm 0.06) \times 10^{-6}$ A/V$^{\frac{3}{2}}$, and the more recent one shows a perveance of $(4.25 \pm 0.05) \times 10^{-6}$ A/V$^{\frac{3}{2}}$. These two values of perveance from two data sets taken at different times are consistent within uncertainty. Note that both data sets show the fitted curve above the data points for higher voltages. We can interpret this by considering two aspects. One is that the uncertainty in current increases as voltage increases, and since the weight is the square of uncertainty reciprocal, the fitting is weighted more towards lower voltage than higher voltage. Moreover, the deviation of the fit from the measurements at higher voltage tells us that as we increased voltage, we were pushing towards the temperature limited regime, where increasing voltage does not have an effect on cathode yield current. In this region, we can see that the current tends to level up at the high voltage end. This can be further explained by looking at the residual plots in the bottom. In both residual plots, we can see a systematic trend that the residual becomes negative at a certain voltage, and then continues to become more negative as voltage increases. What is also

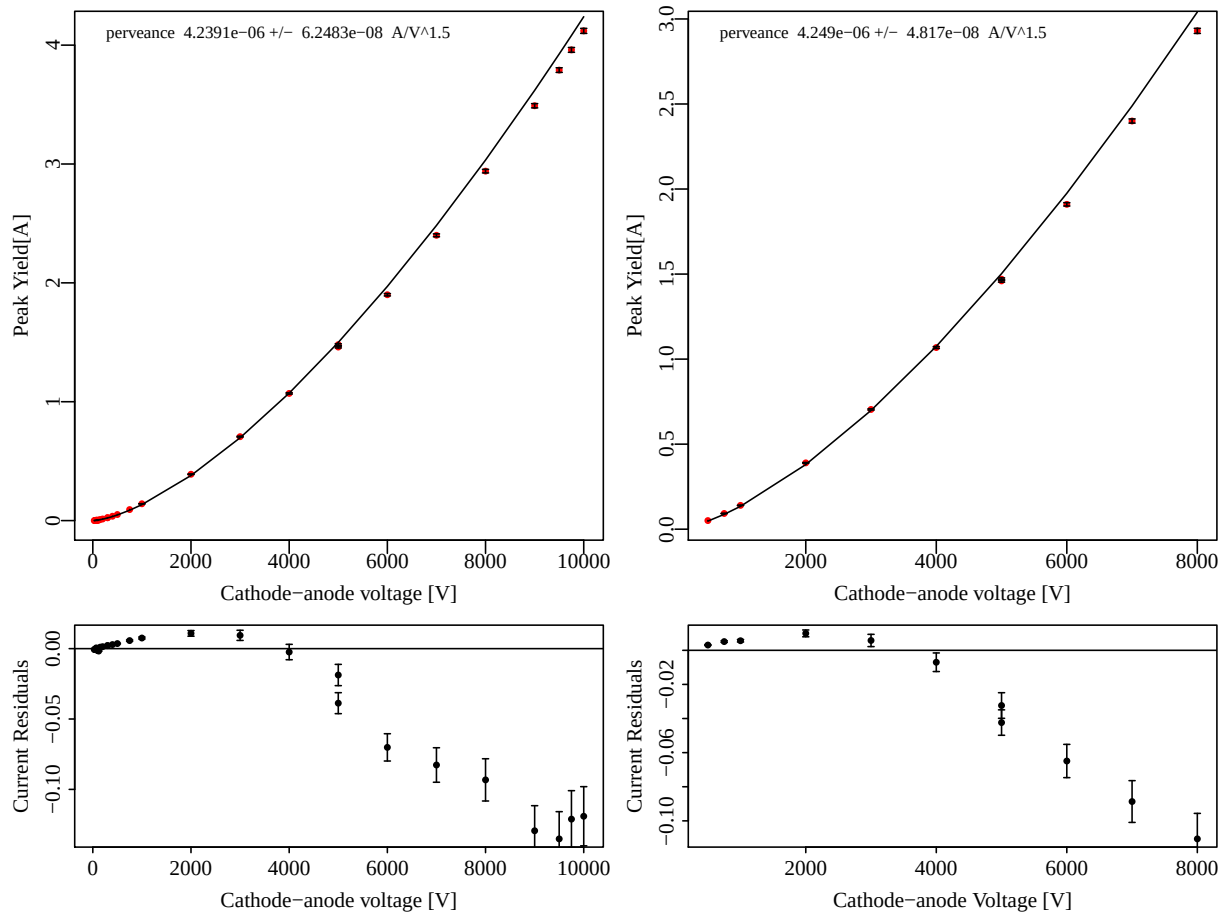

FIG. 9: Perveance analysis using data from December, 2011 - February, 2012 (left), and June, 2012 (right). Top are perveance measurements. Below are residuals.

interesting is that in the residual plots, we see that at low voltages, the residuals are systematically positive. This can be explained by the imperfect vacuum inside the solenoid. In the low voltage region, electrons have lower energy. Because of the presence of rest gas inside the solenoid, electrons with lower energy are more likely to interact and ionize with the gas molecules and get partially neutralized. Therefore, the collector takes in more electrons than predicted.

D. Cathode Yield vs. Temperature

To study the relation between cathode yield current and temperature, we first calibrated temperature against the resistance of the heating filament. The filament resistance is calculated using Ohm's law, $R = \frac{V}{I}$, taking the filament voltage and filament current. Figure 10 illustrates the relation. The vertical line is what we took the temperature to be 1100 °C, corresponding to the filament current of 8.75 A. When the filament is at room temperature, we measured its voltage and current to get its resistance at 300 K. Assuming a

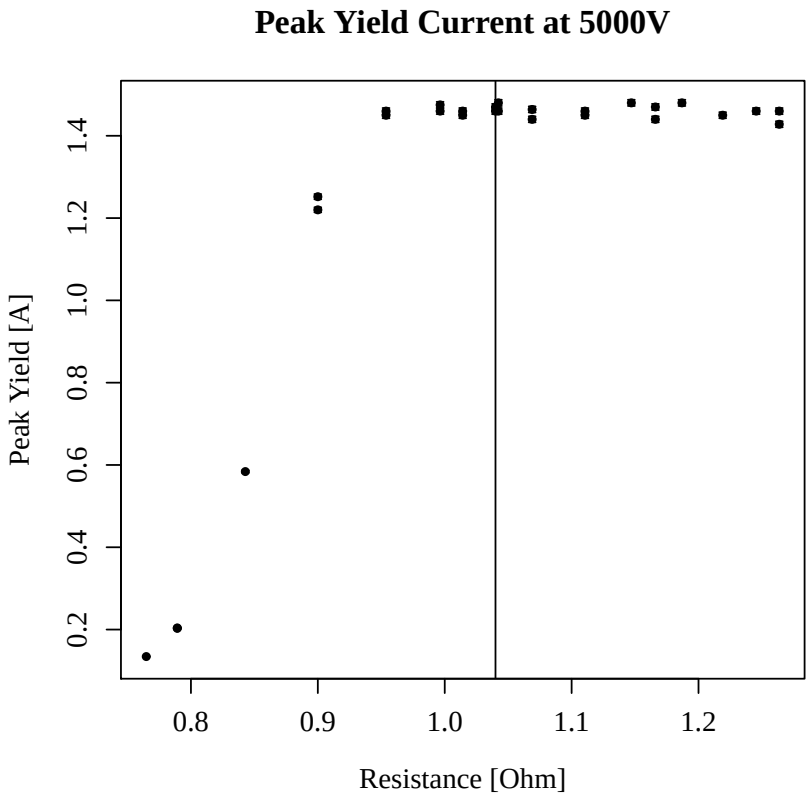

FIG. 10: Peak yield current as a function of filament resistance, keeping the voltage fixed at 5000 V

linear relation between temperature and resistance, we are able to calibrate temperature against filament resistance. Figure 11 illustrates the linear relation between temperature and resistance. The calibration result is $T(\mathrm{K}) = 1795.7R(\Omega) - 462.29$.

Using this calibration, we are able to study how temperature is involved in the cathode emission. Figure 12 shows the peak yield current as a function of temperature. The data points in this plot were taken when the voltage equals 5000 V. We see that below a certain temperature, the current seems to increase exponentially as temperature increases. This region corresponds to the temperature-limited regime, which can be described by Richardson-Dushman equation corrected for Schottky effect. Once the temperature reaches a certain value, the current levels up and stops increasing. The flat area corresponds to the space-charge limit region, where the increase in current is independent of temperature. This regime can be described by Child-Langmuir equation.

As mentioned Section [II], Longo proposed a model to describe the transition between the space-charge limited regime and the temperature limited regime. Bearing this in mind, we attempted to fit our data with

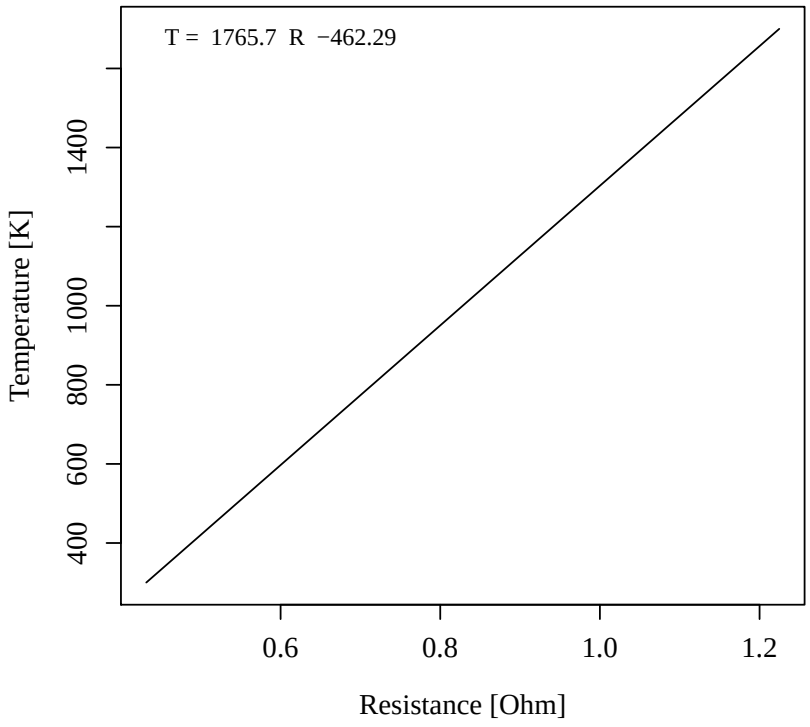

FIG. 11: Calibration between temperature and resistance.

Longo's model. With some algebraic manipulation, Eq. 7 can be written as follows,

$$I_{op} = a[(\frac{1}{J_{sc}})^{\alpha} + (\frac{1}{J_{tl}})^{\alpha}]^{-\frac{1}{\alpha}}, \tag{10}$$

where I_{op} is the measured cathode current, a is the effective cathode area, and J_{sc}, and J_{tl} are described by Eq. 4 and Eq 2, repeated here:

$$J_{sc} = \frac{PV^{\frac{3}{2}}}{a}, \tag{11}$$

$$J_{tl} = A_0 T^2 e^{-\frac{e}{kT}\left[\phi - \sqrt{\frac{eV}{4\pi\varepsilon_0 d}}\right]}, \tag{12}$$

where ϕ is the work function of the cathode surface, and d is the effective distance between the cathode and the anode. There are 6 parameters: a, α, d, A_0, P, ϕ. a and d can be found from Figure 6, which gives $a = 3.6 \times 10^{-4}$ m^2 and $d = 1 \times 10^{-2}$ m. We expect the effective area and distance to slightly deviate from the calculated values because beam dynamics and electrode effects are not considered in calculation above. We expect the perveance P to be on the order of 4×10^{-6} A/V$^{\frac{3}{2}}$. We expect the shape factor α to be approximately one, as the case for typical cathodes. For starting, we set one parameter free at a time, while

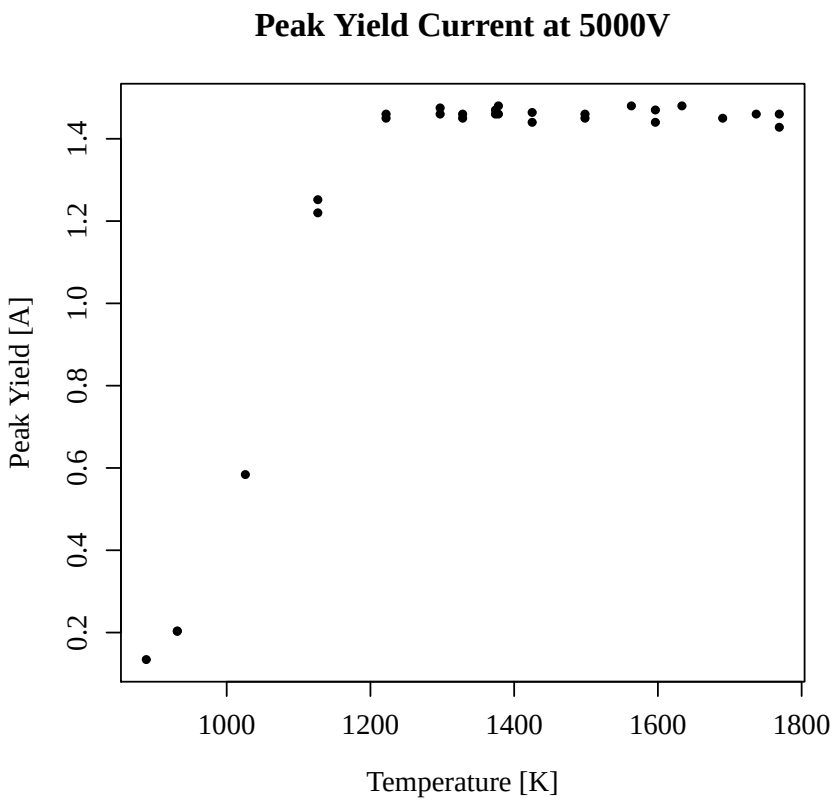

FIG. 12: Peak yield current as a function of temperature, keeping the voltage fixed at 5000 V

fixing the other parameters at expected values. Next, we let two parameters free and repeated the previous step. In doing so, we finally found out that the maximum number of free parameters this model can take before diverging is 3, in terms of three combinations: a, α, P, or α, P, A_0, or α, P, ϕ. That the model cannot fit more than three free parameters makes sense because some of the parameters are correlated with each other, and it is impossible for the model to fit correlated parameters simultaneously. we chose the third combination of the three parameters and fixed them with the fitting results. Then we individually fitted the other parameters. Table I shows the result.

We have assumed a linear relation between heating filament resistance and temperature for the temperature calibration, denoted by $T = \beta R + T_0$. In the previous fitting, we have fixed the two parameters β and T_0 by setting the correspondence between minimum/maximum resistance and room temperature/operating temperature. Leaving the two parameters free, we got consistent results with $\beta = (1765.694 \pm 1.106)$ K/Ω and $T_0 = (-461.722 \pm 0.998)$ K. This consistency indicates the validity of assuming a linear relation between temperature and resistance.

Figure 13 illustrates the fitting. The curves represent the fitted models corresponding to different voltage,

TABLE I: Fitting results of Longo's model

Free parameter	Results
α	1.224 ± 0.039
P	$(4.156 \pm 0.015) \times 10^{-6}$ A/V$^{\frac{3}{2}}$
ϕ	(1.2613 ± 0.0015) eV
a	$(7.443 \pm 0.122) \times 10^{-4}$ m^2
d	$(1.432 \pm 0.15) \times 10^{-2}$ m
A_0	(1024.00 ± 32.64) A/m^{2}K^2

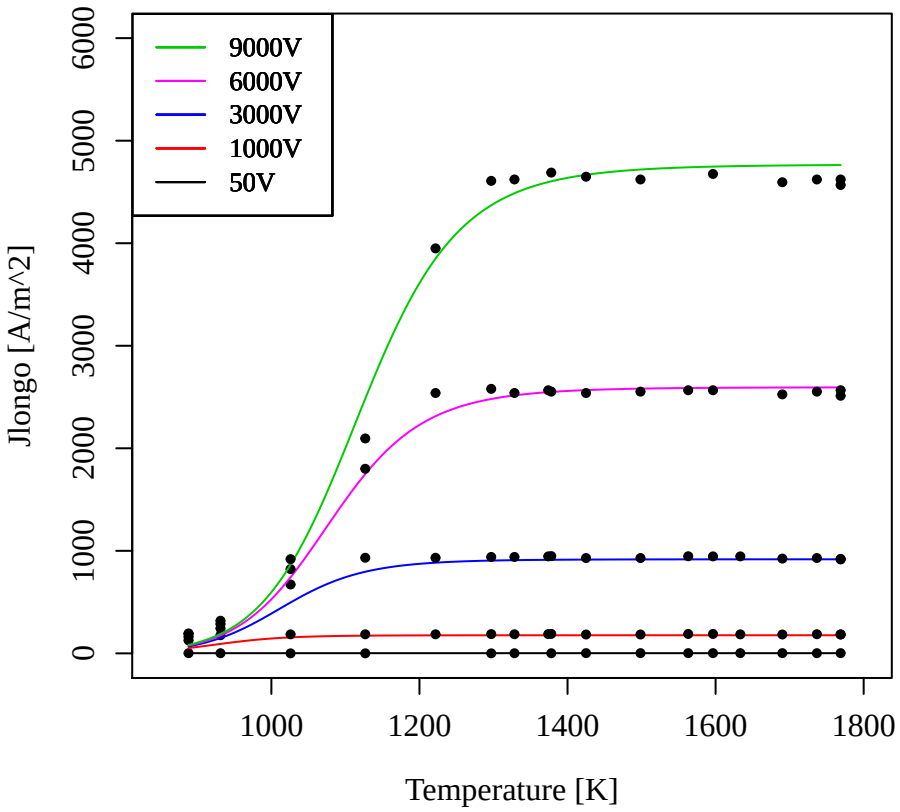

FIG. 13: Fitting results of Longo's model

and the points represent measurements.

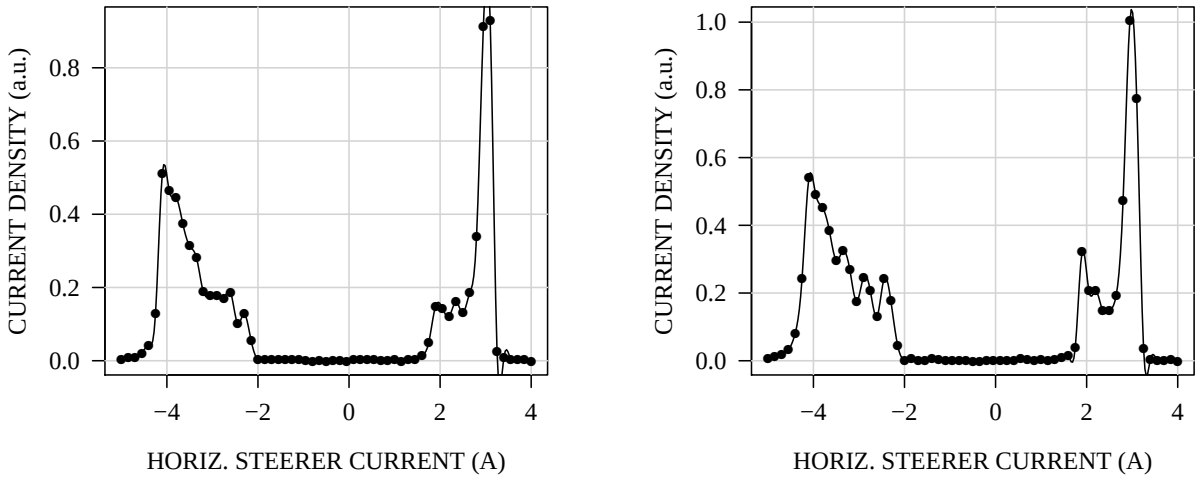

FIG. 14: 1D horizontal scan of hollow electron beam taken at 8 kV. January 2012 (left). June 2012 (right).

E. Beam Profile Measurements

We also did some profile measurements of the hollow electron beam at different voltages. Figure 14 compares the horizontal cross section of the hollow electron beam, taken at different times. Both plots show that the current density is higher on the right than that on the left. Figure 15 compares the 2 dimensional cross section of the hollow electron beam taken at different times. We can see that the current density is stronger at the vertical edges and in the positive horizontal direction than that in the negative horizontal direction. The unsymmetrical pattern shown above can be explained by either off-concentricity of the cathode with respect to the extraction electrode, or an unsymmetrical distribution of the solenoid magnetic field. For the latter possibility, we would expect to see different level of unsymmetry at different currents. However, we have repeated the profile measurement at different currents, and the profiles show the same unsymmetry, which helped us eliminate the second possibility. The tolerance on concentricity becomes harder to achieve as we use larger and longer cathode. This 1-inch hollow electron gun is the largest and longest cathode we have used so far.

After we have diagnosed the off-concentricity of the cathode with respect to the extractio electrode, we took out the electron gun from the Electron Lens Test Stand and disassembled different components of the gun. We measured the distance between the cathode and the electrod to be (0.4 ± 0.2) mm. The gun was sent to Fermilab Mechanical Support Department for cleaning. The concentricity has improved to (0.40 ± 0.05) mm. Reassembly of the gun is currently in progress.

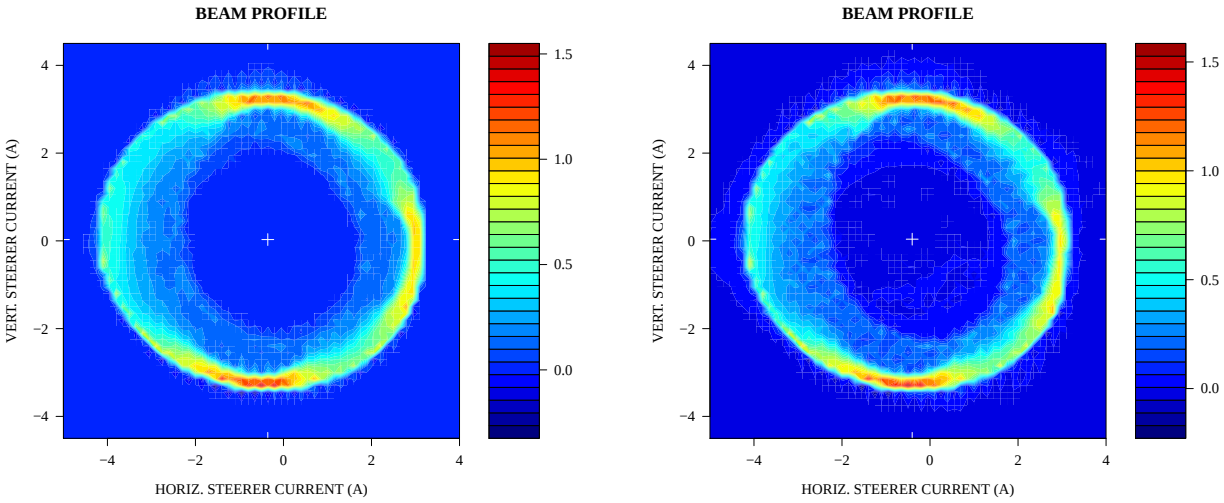

FIG. 15: 2D horizontal scan of hollow electron beam taken at 8 kV. January 2012 (left). June 2012 (right).

V. CONCLUSION

In conclusion, we have measured the characteristics of a new 1-inch electron gun. We have covered two major characteristics, namely the cathode yield as a function of cathode-anode voltage and as a function of cathode temperature, and beam profile. The perveance measurement illustrated the relation between cathode yield current and cathode-anode voltage. We chose to extrapolate perveance at a working temperature close to space-charge limited regime. The measurements taken in early 2012 and June 2012 show consistent results. The Longo model fitting illustrated the relation between cathode yield current and cathode temperature. We made use of all data taken at various temperatures and cathode-anode voltages, including both space-charge limited and temperature limited regimes. The fitting results showed effective parameters that characterize the electron gun. The beam profile measurements taken in early 2012 and June 2012 consistently show an imperfect concentricity of the cathode in relation with the anode. Thus, we have identified a cathode off-center problem and the electron gun has been sent to related facilities for improvements.

In the future, we will repeat the characterization measurement to see the change in cathode yield and beam profile from the improved electron gun geometry.

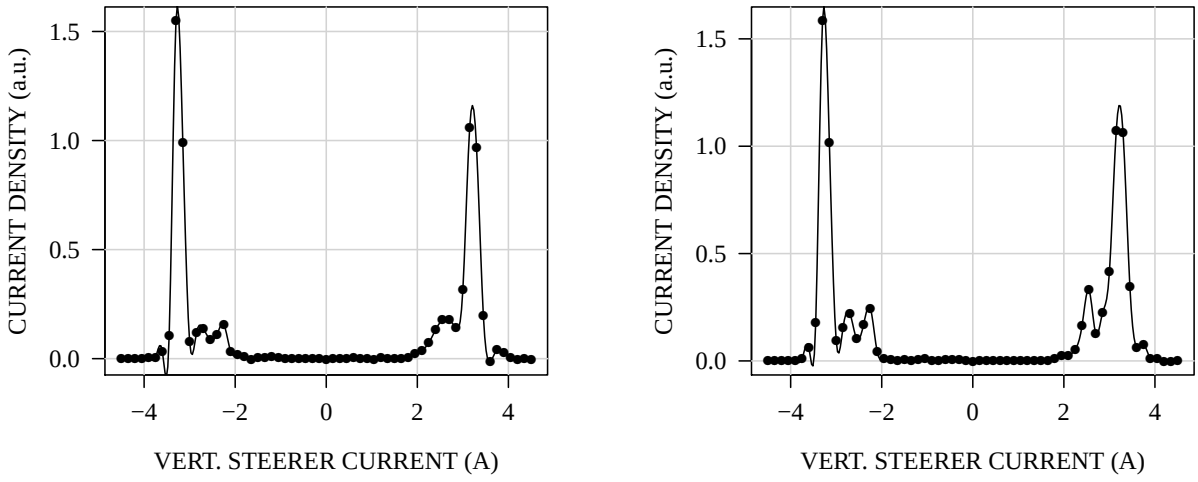

FIG. 16: 1D vertical scan of hollow electron beam taken at 8 kV. January 2012 (left). June 2012 (right).

APPENDIX A: ORGANIZATION OF WORKING DIRECTORY

My working directory is lisiqi@mrbutts.fnal.gov. The home directory consists of the following sub-directories: /ana for analysis, /report for report, and /data for data. The analysis directory contains all the R scripts to produce the fitting results and plots presented in this paper. Produced plots are saved in the nested directory /plots under /ana. The report directory contains all drafts that composes this paper, including the original tex files and compiled pdf files. A subdirectory /template nested under the report directory contains all the formatting information for composing this report. The data directory contains all measurements data related to this paper, including measurements taken from January, February and June 2012. Figures that illustrate the physical appearance of experimental apparatus, including gun geometry diagram, are also saved in the data directory. There is also an /old_version directory nested under data and analysis directory, which saves obsolete data, plots and R scripts.

APPENDIX B: SUPPLEMENTARY MATERIALS

In Section [IV], we have shown the one-dimensional scan from the horizontal direction. Here we show the one-dimensional scan from the vertical direction, comparing measurements taken in early 2012 and June 2012 in Figure 16.

Figure 17 shows the filament resistance change as a function of filament current. Filament resistance is determined by dividing filament voltage by its current.

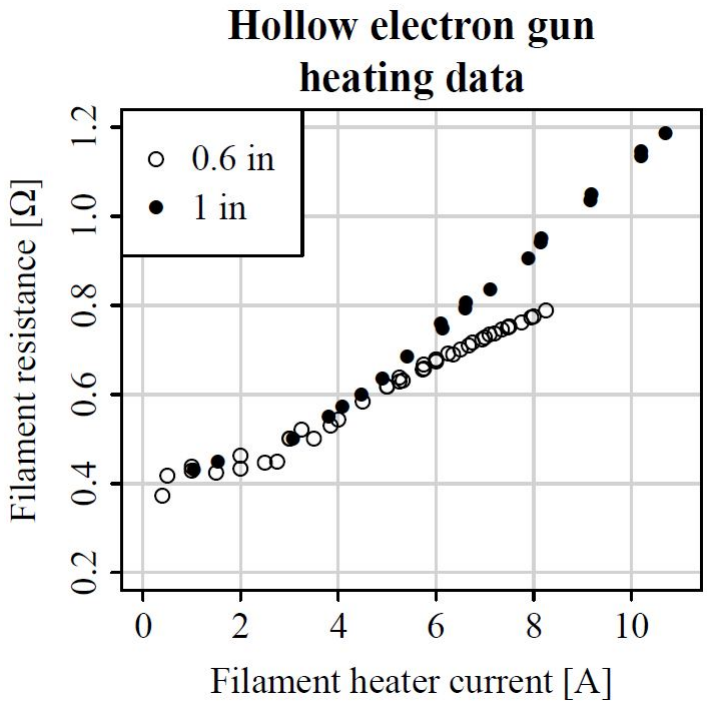

FIG. 17: Filament resistance as a function of filament current for 0.6-inch and 1-inch electron gun respectively.

[1] A. J. Lichtenberg and M. A. Lieberman, *Regular and Chaotic Dynamics* (Springer-Verlag, New York, 1992), p. 320.

[2] G. Stancari, Phys. Rev. 107, 084802 (2011).

[3] G. Stancari et al., Proc. 2011 Part. Accel. Conf.(PAC11), New York, NY, USA, pp. 370 - 372; G. Stancari et al., Proc. 2011 Int. Part. Accel. Conf.(IPAC11), San Sebastian, Spain, pp. 1939 - 1941; G. Stancari et al., Proc. 2012 Int. Part. Accel. Conf.(IPAC10), Kyoto, Japan, pp.1698 - 1700.

[4] A.S. Gilmour, Jr., in *Principles of Traveling Wave Tubes,* Norwood, MA, 1994, pp. 53.

[5] R.T.Longo, "Physics of Thermionic Dispenser Cathode Aging," Journal of Applied Physics, Volume 94, Number 10, pp. 6966 - 6975.

[6] R.Vaughan, IEEE Trans. Electron Devices **ED-33**, 11, 1986.